Available online at www.sciencedirect.com
SCIENCE DIRECT
International Journal of Mass Spectrometry 247 (2005) 72–80
International Journal of Mass Spectrometry
www.elsevier.com/locate/ijms

A hollow cathode proton transfer reaction time of flight mass spectrometer

C.J. Ennis, J.C. Reynolds, B.J. Keely, L.J. Carpenter *

Department of Chemistry, University of York, Heslington, York, YO10 5DD, UK

Received 19 July 2005; received in revised form 28 September 2005; accepted 29 September 2005
Available online 2 November 2005

Abstract

A proton transfer reaction mass spectrometer has been developed that couples a readily portable hollow cathode proton transfer reaction cell with a reflectron time of flight detector (PTR-ToF). The instrument is capable of detection of trace gas components as low as 1 ppbv on a timescale of between 10 and 60 s and with a sensitivity of 3.7 ncps $ppbv^{-1}$ (normalised counts per second per parts per billion by volume) for toluene and 28 ncps $ppbv^{-1}$ for acetone. The PTR-ToF instrument developed is capable of high mass resolution, high mass accuracy (∼300 ppm) and multiplexed spectral acquisition, leading to rapid and selective online analysis of trace components in complex gas mixtures. Attention to the materials chemistry of the system and the reaction conditions in the PTR cell are expected to enable the detection limit of this instrument to be lowered and the sensitivity enhanced.

Keywords: Proton transfer reaction mass spectrometry; Atmospheric analysis; Time of flight mass spectrometry

1. Introduction

Proton transfer reaction mass spectrometry (PTR-MS) has been used for almost a decade as a fast online technique for detection and analysis of trace hydrocarbons in gaseous samples [1–11]. Major applications of the technique are in breath analysis and atmospheric chemistry, and detection limits as low as a few pptv are routine [10,11]. The technique relies on chemical ionisation by gas phase proton transfer to produce protonated molecules with little or no fragmentation, facilitating the analysis of complex gas mixtures without the need for a separation step in the analytical method.

In PTR-MS, proton transfer is usually achieved using gas-phase hydronium ion (H_3O^+) as the protonating agent:

$$H_3O^+ + R \rightarrow RH^+ + H_2O \quad (1)$$

where R is a gas phase analyte. The proton affinity of R, PA(R) is defined as

$$PA(R) = -\Delta H \quad (2)$$

for the above reaction, and is simply a measure of the exothermicity of the gas phase proton transfer. Molecules with a PA greater than that of gas phase water are readily protonated by the hydronium ion, with rate constants approaching the collisional limit. For small molecules, differences in PA are small compared to dissociation energies of the protonated ions, so soft chemical ionisation occurs with little or no fragmentation. Thus, PTR-MS produces a protonated molecule for each gas phase component that is capable of undergoing protonation. This includes most oxygenated organic molecules and a large number of hydrocarbons that possess more than four carbon atoms. A specific advantage of the technique is that only the trace components of the air are protonated, the proton affinity of molecular oxygen, carbon dioxide, molecular nitrogen and other main components of air being lower than that of water. Thus, the technique represents a fast, sensitive and selective method for analysing components of air that are of considerable interest to atmospheric scientists.

Quantification in PTR is possible via knowledge of the protonation rate constants [1], which are known for many species [12,13]. However, a failing of the method as both a qualitative and a quantitative analytical tool lies in the mass spectrometric detection technology. Typically, quadrupole mass spectrometers (QMS) are used in PTR-MS; consequently, the mass resolution is limited. This results in a lack of discriminating power between nominally isobaric materials, that is, between non-isomeric materials with the same nominal molecular mass. Strategies to overcome this problem include the use of different protonating

* Corresponding author. Tel.: +44 1904 434588; fax: +44 1904 432516.
E-mail address: ljc4@york.ac.uk (L.J. Carpenter).

1387-3806/$ – see front matter © 2005 Elsevier B.V. All rights reserved.
doi:10.1016/j.ijms.2005.09.008

agents (e.g., NH_4^+) and the alteration of proton transfer collision energetics [5], though these techniques are not ideal for online-analysis. Recent work to develop an ion trap PTR instrument has made some progress towards addressing this drawback [14]. In the ion trap, ion-neutral collisions can be induced to promote fragmentation, and multistage tandem MS enables differentiation between isobaric molecules for example methacrolein and methyl vinyl ketone [14].

An alternative strategy is to use a time of flight (ToF) mass spectrometer to analyse the protonated molecules produced in the proton transfer reaction flow drift tube. ToF mass spectrometry has the potential to benefit over QMS in this application for two reasons. Firstly, the generally higher mass resolving capability of the technique can provide elemental composition leading directly to discrimination between nominally isobaric analytes. The second advantage is an increased spectral acquisition rate that is expected to lead to higher sensitivity.

Recently, the capabilities of PTR-ToF using a radioactive ionisation source (^{241}Am, 1.2 mCi) have been demonstrated [15] with linearity of detection in the range 3–53 ppmv giving inferred detection limits in the ppbv range over integration times of around 1 min. Here we demonstrate PTR-ToF capability using a hollow cathode ionisation source with limits of detection below 10 ppbv for integration times of 10–60 s.

2. Experimental

The PTR-ToF developed at York comprises an aluminium flow drift tube interfaced to a custom built R500 time of flight mass spectrometer (KORE Technologies, Ely, UK) and is shown schematically in Fig. 1. The instrument requires a 1 m × 2 m footprint, weighs ∼300 kg, and has an average power requirement of 3.4 kW. Primary hydronium ions are produced in a tungsten hollow cathode interfaced to a short source-drift (SD) tube in which hydronium ion production is maximised by ion-neutral reactions with water vapour [1]. The ions pass forward into the flow-drift tube (FDT) which consists of a stack of four aluminium drift rings with internal diameters of 50 mm and two thinner lensing rings at the top and bottom of the FDT. The overall length of the tube is around 75 mm and the tube is bounded by a 1 mm injection orifice and a 500 μm extraction orifice.

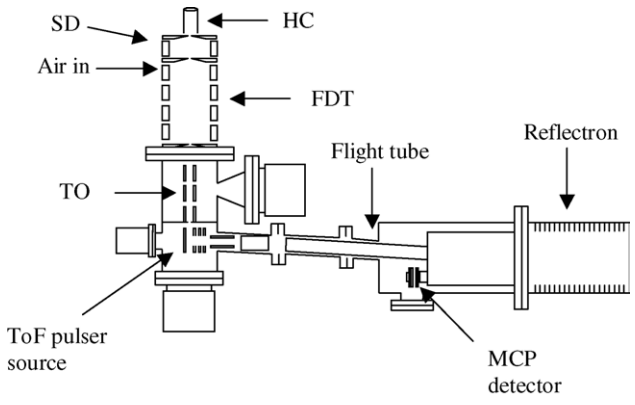

Fig. 1. PTR ToF schematic, showing the hollow cathode (HC) ion source, source drift (SD) tube, flow drift tube (FDT), transfer optics (TO) into the ToF pulser source, field free flight tube, reflectron and microchannel plate detector (not to scale).

Within the FDT, proton transfer reactions occur between hydronium ions and protonatable analytes. The total ion yield is passed through the FDT extract orifice and directed to the pulse source of the ToF via the transfer optics (TO) in the pressure step region. Perpendicular pulse-out of ions is effected in the ToF source.

The ToF consists of an R500 reflectron ion mirror pumped by a 100 L s^{-1} turbo with an operating base pressure of 10^{-7} mbar. Ion detection is by a microchannel plate detector. The system is operated by purpose written software operating in a Grams GUI environment.

The design of the FDT was informed by ion trajectory modelling using SIMION [16]. The effect of pressure in the drift tube was modelled in various ways, including the viscous drag model provided with SIMION. Further pressure models were constructed using SIMION's built in programming language, RPN. These included a model to impose a calculated drift velocity on the flying ions. The most sophisticated implementation of this model calculated the ion speed according to the pressure and field gradient:

$$v_d = \mu E' \tag{3}$$

where v_d is the ion drift velocity, μ is the ion mobility and E' is the electric field gradient in the direction of ion travel at the beginning of each time-step, given by:

$$|E'| = \frac{\vec{E} \cdot \vec{V}}{|V|} \tag{4}$$

in which $\vec{E}$ and $\vec{V}$ are the three dimensional electric field and ion velocity vectors, respectively. The product is readily handled using RPN's unit vector functions.

Breakdown of the linear proportionality between the drift velocity and the reduced field occurs at fields higher than around 10 V cm^{-1} Torr (for ions) [17]. In models this breakdown leads to un-realistically large drift velocities at high fields. To avoid this condition, drift velocity can be modelled by the parabolic relationship [17]:

$$v_d = \left(\frac{\delta}{2}\right)^{1/2} \left(\frac{Ee\lambda_m}{m}\right) \tag{5}$$

where e is the electronic charge, λ_m is the mean free path of gas particles and m is the mass of the gas particles. The average fraction of the ion's energy transferred during collision, δ, is given by:

$$\delta = \frac{2m_1m_2}{(m_1 + m_2)^2} \tag{6}$$

This parabolic dependence of v_d on E/p (where p is the drift tube pressure, proportional to $1/\lambda_m$) is approximately linear at low values of E/p and prevents unrealistic large velocities occurring at high fields.

All the various models display the same general features (Fig. 2). Ions enter the drift tube and are subject to so-called collisional focussing [18] as a result of interaction with neutral

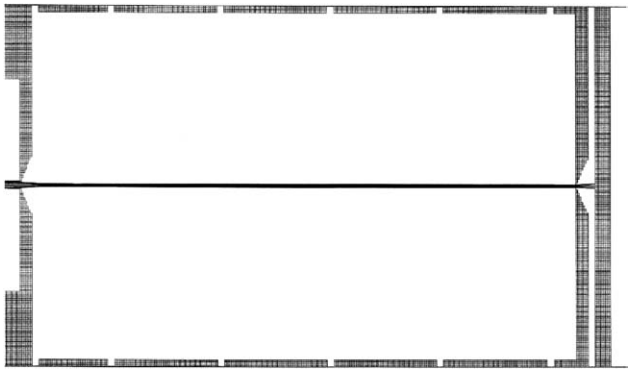

Fig. 2. Calculated path of ions through drift tube, using RPN code to simulate effect of high pressure. See text for details.

species. The resultant ion beam is tightly focussed along the longitudinal axis of the FDT.

3. Results and discussion

3.1. Distribution of primary ions in the FDT

Our first generation PTR-ToF operates with a drift tube pressure of 0.6–1.0 mbar and a 240 V dc potential difference between injection and extraction orifices. The simple orifice design in this drift tube leads to relatively high humidity as a result of forward transport of water from the primary ion source into the drift tube. Because of this high humidity, we operate the FDT at relatively high values of reduced-field (E/N, where E is the electric field across the FDT and N is the gas number density). A plot of the distribution of primary protonating ions as a function of reduced field (Fig. 3) reveals that the hydronium ion essentially dominates the ion source output at reduced field values in excess of 120 Td (where 1 Td = 1 Townsend = 10^{-17} V cm^2).

High reduced-field values lead to collision induced fragmentation of secondary ions in PTR-MS. Therefore, further reductions in reduced field are required in order to suppress fragmentation and make available the full utility of the PTR-ToF technique. The distribution of primary protonating ions in the drift tube is a function of both reduced field and relative humidity of the buffer gas. In our instrument, the high water vapour loading of the buffer gas drives the water cluster formation equilibrium

$$H_3O^+ + H_2O \rightleftharpoons (H_2O)_2H^+ \quad (7)$$

further to the right hand side, leading to the formation of significant levels of hydrated hydronium ions at relatively highly reduced fields.

A strategy for improving the first generation PTR-ToF would be to effect a reduction in FDT humidity. This would shift the cluster ion distribution in the direction of lower reduced field in Fig. 3. A possible solution is simply to operate at higher buffer gas pressure, thereby reducing the relative humidity. Further improvements resulting from such an increase in operating pressure are discussed in Section 3.3. Since back-diffusion of air dilutes the water vapour in the SD region, hampering the formation of hydronium ions from the initially formed H_2O^+, a further improvement in performance should be gained by introducing a venturi inlet at the injection orifice in order to limit the amount of back-diffusion into the SD region.

During operation of the FDT with N_2 carrier gas (zero grade, BOC), the hydronium yield is the primary output ion and the cationic dioxygen signal is weak (Fig. 4). When air (zero grade, BOC) is used as the buffer gas in the FDT, the amount of hydronium ion falls and that of ionised dioxygen rises. This indicates that significant back diffusion of gas load from the FDT to the ion source occurs. When the buffer gas is nitrogen, back-diffusion dilutes the water vapour feed to the hollow cathode and decreases the number density of reactants in the SD. Both of these effects are deleterious with regard to absolute hydronium ion yields. However, the situation is worse still when the buffer gas is air (containing oxygen). In this case, oxygen entering the hollow cathode is ionised in competition with water vapour. For a given current density in the hollow cathode plasma, dioxygen ions compete as charge carriers with ions derived from water vapour. This significantly reduces the yield of hydronium ions from the high-density hollow cathode plasma. Reduction of back-diffusion of carrier gas by installation of a venturi inlet is, therefore, expected to increase the sensitivity of PTR-ToF by limiting the dilution of species in the SD region and

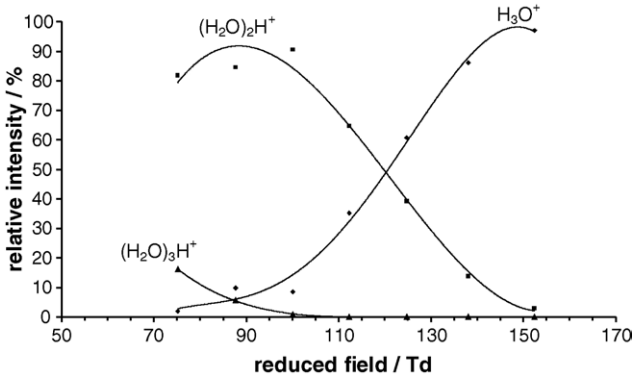

Fig. 3. PTR-ToF primary protonating ion distribution as a function of reduced field.

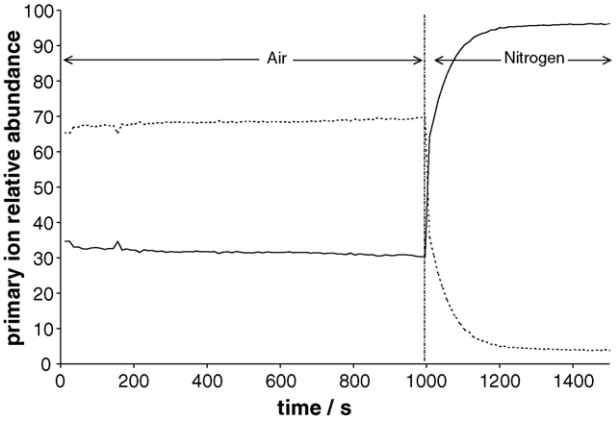

Fig. 4. Relative distribution of O_2^+ and H_3O^+ ions as a function of buffer gas identity. Solid line represents H_3O^+ relative abundance; broken line represents O_2^+ relative abundance.

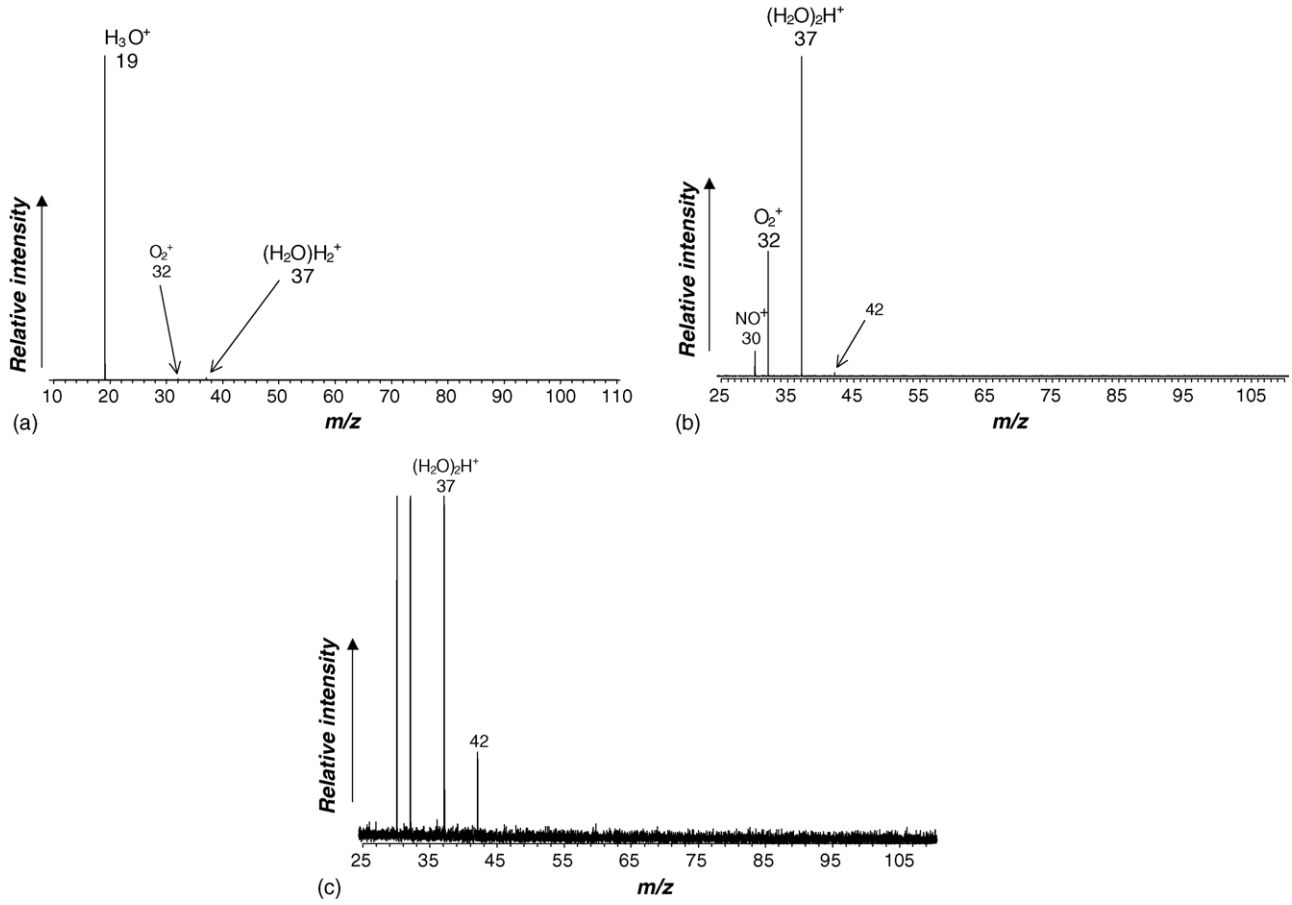

Fig. 5. PTR-ToF spectrum obtained using nitrogen from the headspace of liquid nitrogen as the working fluid in the PTR: (a) shows the full scan, displaying the strong signal from hydronium ion; (b) shows the NO^+, O_2^+ and $(H_2O)_2H^+$ ions produced in the PTR-ToF experiment; (c) shows a magnified view of the mass spectrum above $m/z = 30$ to display the features in the background of the instrument.

by maintaining a high hydronium precursor charge carriers in the HC.

3.2. PTR-ToF analysis of air and standard gas mixtures

A typical PTR-ToF spectrum (Fig. 5(a)), obtained with the drift tube operating at around 800 μbar and 240 V with nitrogen from the headspace of liquid nitrogen as the buffer gas, shows a strong signal at $m/z = 19$, corresponding to hydronium ion. Other signals are present at $m/z = 30$, 32, 37 (Fig. 5(b)) due to NO^+, O_2^+, and $(H_2O)_2H^+$. The weak signal at $m/z = 42$ is a system contaminant, possibly protonated acetonitrile from o-ring materials on gas handling systems. Fig. 5(c), in which the peaks at $m/z = 30$, 32 and 37 have been truncated to bring the baseline noise on scale, demonstrates that no other ions above $m/z = 30$ are present in the spectrum.

A typical PTR-ToF spectrum (Fig. 6(a)) obtained with the drift tube operating at around 800 μbar and 240 V with laboratory air as the buffer gas shows a strong signal at $m/z = 19$, corresponding to H_3O^+. However, the base peak in this spectrum is due to O_2^+, at $m/z = 32$, of which the hydronium peak is around 80%. Also present in this spectrum are peaks at 30 Th, corresponding to NO^+, and 37 Th, representing the first hydrate of hydronium $(H_2O)_2H^+$. The $m/z = 37$ peak is below 3% of the intensity of the hydronium ion signal at mass 19.

Fig. 6(b) shows a close-up of the mass spectrum in Fig. 6(a), from $m/z = 36$ upwards. The hydrated hydronium ion signal at $m/z = 37$ is truncated in order to bring all less intense spectral features on scale. There is a relatively intense peak at $m/z = 46$, with about 10% the intensity of the mass 37 hydrated hydronium ion peak. This corresponds to the NO_2^+ ion, formed from reaction of O_2^+ with N_2. Several other peaks are present, with considerably less intensity than the NO_2^+ ion—no signal occurs in the mass spectrum above 37 Th with an intensity greater than 10% of the $m/z = 46$ signal. Above $m/z = 62$ the spectrum exhibits no detectable signals.

Fig. 6(c) shows an expanded view of the 38–65 Th range of this spectrum. The signal at $m/z = 46$ is truncated in order to bring all the features more clearly on scale. The intense peak at 39 Th is a due to the $(H_2{}^{18}O)(H_2O)H^+$ isotopomer of hydrated hydronium. Along with this peak, three other peaks in this spectrum can be readily attributed to ionised clusters: $m/z = 48$ is due to the adduct $NO^+ \cdot H_2O$ and $m/z = 50$ is due to $O_2^+ \cdot H_2O$. The small peak at $m/z = 62$ is the smallest signal in the spectrum and is due to the electrophilic adduct $NO^+ \cdot O_2$. The other peaks in Fig. 6(c) are due to chemically ionised species resulting

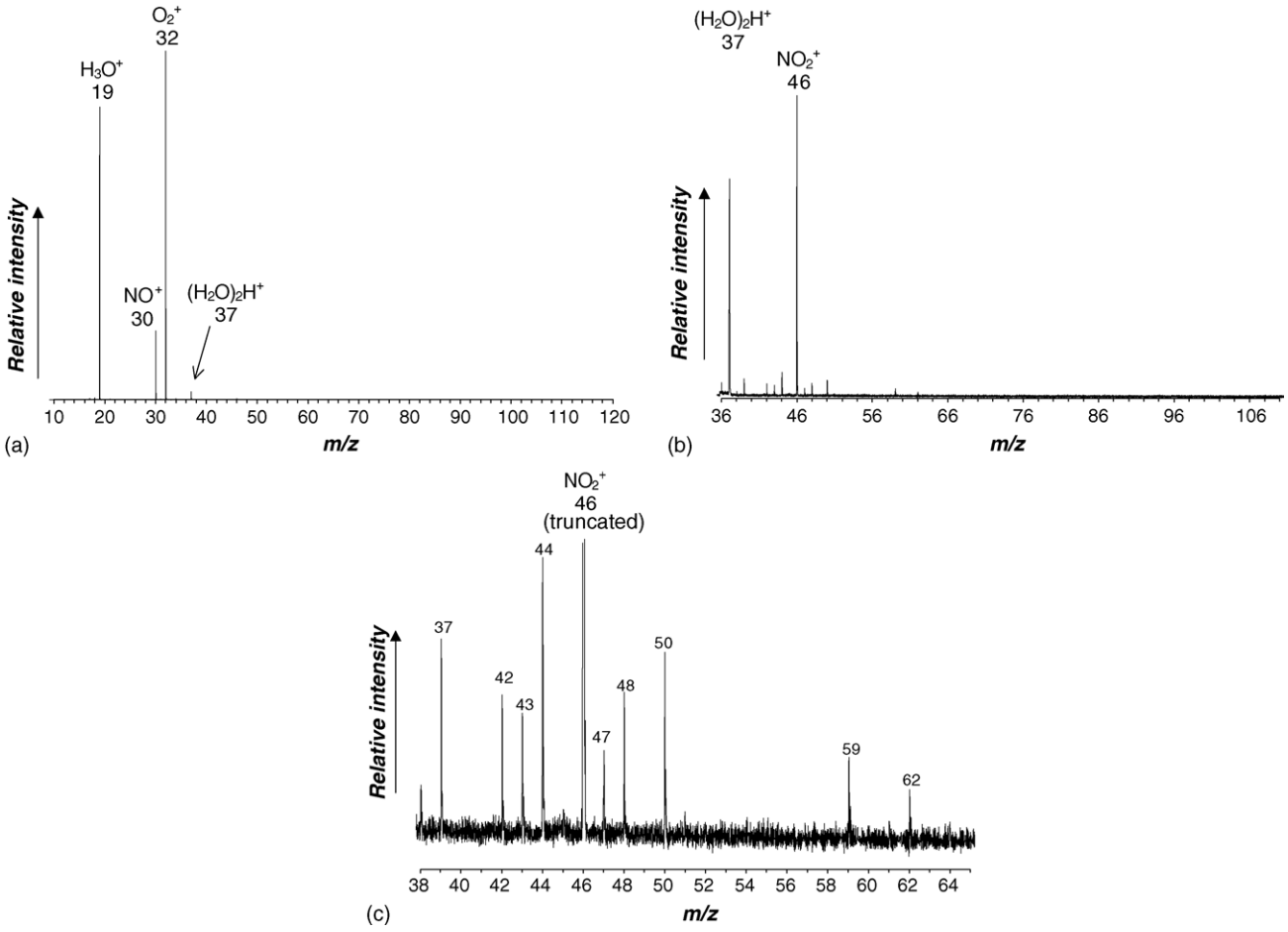

Fig. 6. PTR-ToF mass spectrum of the output of the FDT with air as the buffer gas: (a) shows the full scan, showing strong signals from hydronium ion, dioxygen ion, and protonated water dimer; (b) shows a magnified view of the mass spectrum above 36 Th; (c) shows a magnified view of the mass spectrum between $m/z = 38$ and 65 displaying signals due to cluster formation and to protonation of airborne analytes.

from proton transfer reactions in the drift tube. Of these, the two of highest mass are most readily identified: 59 Th corresponds to $(C_3H_6O)H^+$, most likely due to acetone or propanal; 47 Th corresponds to $(C_2H_6O)H^+$, and is most likely due to ethanol (but see below the discussion of this mass in the spectrum of OVOC standards in nitrogen). The other peaks in the spectrum ($m/z = 42$, 43, and 44) are more challenging to assign. Starting with the most intense of these three ions, $m/z = 44$, it is clear that this may simply represent CO_2^+ ionised in the hollow cathode via back-diffusion of air, or by charge transfer from H_2O^+ formed in the hollow cathode and present in the SD region. Formation of CO_2^+ by charge transfer from O_2^+ is disfavoured by the relatively high first ionisation energy of carbon monoxide. A further possible identity of this ion is the product of collision-induced dissociation of protonated acetone by loss of a methyl radical:

$$[(CH_3)_2CO]H^+ + M \rightarrow [(CH_3)_2CO]H^{+*} \rightarrow [CH_3CO]H^+ + CH_3^\bullet$$

This transition is observed in collision-induced dissociation of protonated acetone in tandem mass spectrometry [19]. The accurate mass measurement (see Section 3.4) for m/z 44 was 44.0476 Th, which is much closer to the mass of $[CH_3CO]H^+$ (44.0526 Th) than to CO_2^+(44.0095), indicating that $[CH_3CO]H^+$ is likely to be responsible for this peak. The peak at $m/z = 43$ is also attributable to a CID process of the protonated acetone precursor [19]:

$$[(CH_3)_2CO]H^+ + M \rightarrow [(CH_3)_2CO]H^{+*} \rightarrow [CH_2CO]H^+ + CH_4$$

The peak at $m/z = 42$ may be the product of protonation of acetonitrile (PA = 779 kJ mol^{-1}).

The full PTR-ToF spectrum of a commercial gas standard containing 50 ppbv of acetone and acetaldehyde in nitrogen (Fig. 7) shows signals at 19 Th (the base peak), 18 Th (H_2O^+), and small signals due to the protonated water dimer at 37 Th, cationic dioxygen at 32 Th, and cationic nitric oxide at 30 Th. The last two ions are of a much-reduced intensity compared with the PTR-ToF spectrum of ambient air, supporting the assignment of these masses to the ions stated.

Protonation of acetone and acetaldehyde gives rise to ions at 59 and 45 Th, respectively (Fig. 8). Notably, the signal at $m/z = 46$ in Fig. 6(b) is almost entirely absent from Fig. 8, supporting the assignment of this ion to NO_2^+. Other notable absences are the

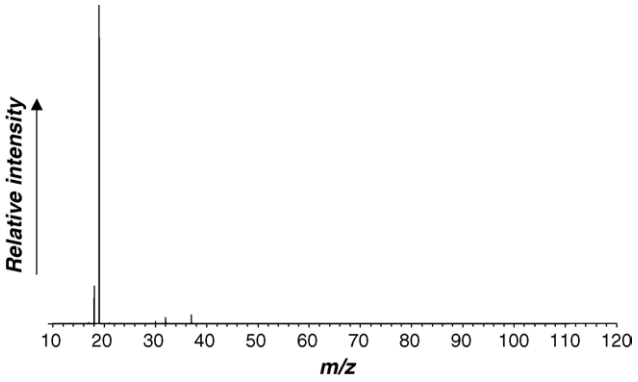

Fig. 7. PTR-ToF mass spectrum of commercial gas standard containing 50 ppbv acetone and acetaldehyde in nitrogen.

electrophilic adduct ions $NO^+ \cdot H_2O$ (48 Th), $O_2{}^+ \cdot H_2O$ (50 Th) and $NO^+ \cdot O_2$ (62 Th), consistent with the absence of oxygen, and further supporting the assignments of these ions. Along with the peak at 59 Th due to protonated acetone, and that at 45 Th due to protonated acetaldehyde, there is a strong signal at mass 44. The absence of air from the drift tube further supports the assignment of this peak to the $[CH_3CO]H^+$ ion formed by collision-induced dissociation of protonated acetone discussed above.

Notably, there is peak in the PTR-ToF spectrum of OVOC/nitrogen standard at mass 61, which is the mass of protonated propanol. However, the absence of propanol from the standard and from the PTR-ToF spectrum of pure nitrogen (demonstrating system cleanliness with respect to propanol) leads to the assignment of this mass to a protonated ketene monohydrate species $[H_2C{=}C{=}O]H^+ \cdot H_2O$:

$$[(CH_3)_2CO]H^+ + M \rightarrow [H_2C{=}C{=}O]H^+ + CH_4 \quad (9)$$

$$[H_2C{=}C{=}O]H^+ + H_2O \rightarrow [H_2C{=}C{=}O]H^+ \cdot H_2O \quad (10)$$

The signal at 47 Th may be due to ethanol, but this is unlikely given the nature of the standard. An alternative explanation is the series of reactions:

$$[(CH_3)_2CO]H^+ + M \rightarrow [C_2H_4]H^+ + H_2CO \quad (11)$$

$$[C_2H_4]H^+ + H_2O \rightarrow [C_2H_4]H^+ \cdot H_2O \quad (12)$$

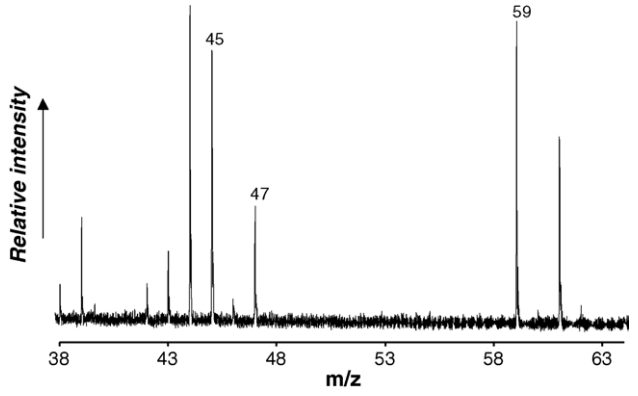

Fig. 8. Magnified view of PTR-ToF spectrum of OVOC standards in nitrogen.

This rearrangement of protonated acetone to protonated ethene is supported by the observation of an ion at mass 29 in the PTR-ToF spectra. Both of the fragmentation processes of protonated acetone shown above, leading to the formation of protonated ketene and protonated ethene, are observed in collision-induced dissociation of protonated acetone in tandem MS [19].

The peak at mass 43 is also attributable to a CID process of the protonated acetone precursor [19]:

$$[(CH_3)_2CO]H^+ + M \rightarrow [(CH_3)_2CO]H^{+*} \rightarrow [CH_2CO]H^+ + CH_4 \quad (13)$$

The peak at mass 42 may be the product of protonation of acetonitrile (PA = 779 kJ mol^{-1}).

This plethora of fragmentation and clustering reactions represents a complicating factor in the analysis of PTR-ToF spectra that needs to be overcome in order to render the instrument capable of analysis of complex atmospheric mixtures on a realistic timescale. Fragmentation is due to high-reduced fields, and the reduction of reduced field is of paramount importance in the construction of PTR-ToF spectrometers [15].

3.3. Sensitivity of PTR-ToF

The response of the PTR-ToF to standard gas concentrations of acetone and acetaldehyde in nitrogen is shown in Fig. 9. An immediate and reversible response is observed for both compounds.

The concentration of analyte molecules in the gas phase can be calculated from the PTR-ToF response via the equation:

$$\frac{I_{RH^+}}{I_{H_3O^+}} = \rho_R \times \frac{kLN^2}{\mu_0 N_0 E} \times R_f \quad (14)$$

where ρ_R is the volume mixing ratio of analyte R in parts per billion by volume (ppbv) and R_f is a response correction factor. At the high, but constant reduced field in our FDT, this response factor takes into account the fragmentation of protonated analytes. This correction factor can be evaluated from standard concentrations and is shown to be 1.47 for acetaldehyde and 2.79 for acetone in our PTR-ToF instrument under the present operating conditions. The evaluated volume mixing ratios for the two standard compounds are:

- acetaldehyde VMR = 50 ± 1.8 ppbv;
- acetone VMR = 50 ± 2.0 ppbv.

The main source of error in these data arises from the uncertainty of the rate constants used for calculating the concentrations of the specific analytes. In the light of the collision-induced fragmentations discussed in the previous section, it is not surprising that the acetone concentration is somewhat lower than that calculated assuming quantitative production of the protonated molecule.

Calibration graphs for the PTR-ToF response to acetone and toluene are shown in Fig. 10. These data were obtained in the case of acetone by using a standard gas mixture diluted with zero grade nitrogen online using mass flow control. The toluene data

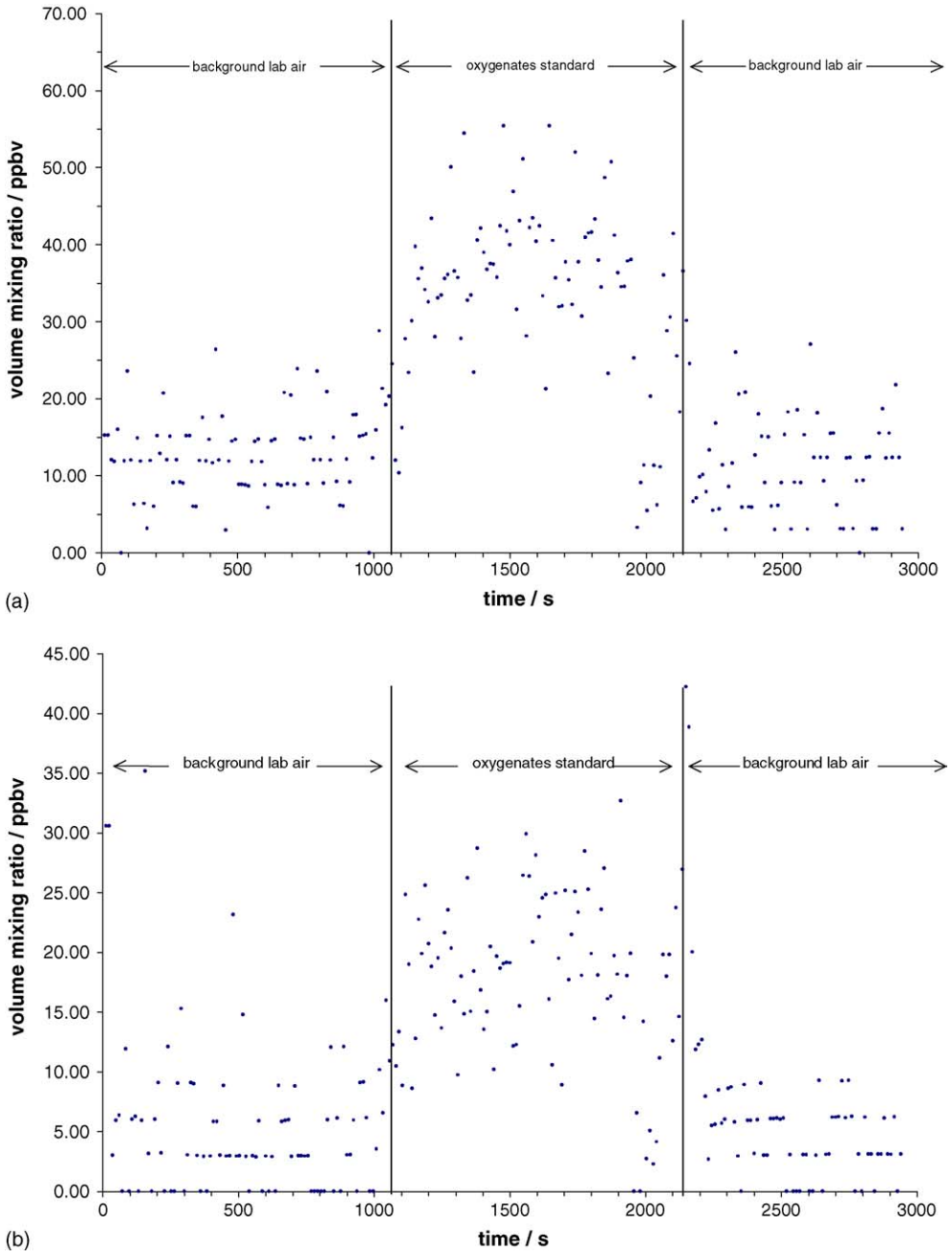

Fig. 9. PTR-ToF response to standard concentrations of (a) acetaldehyde and (b) acetone in nitrogen. Volume mixing ratios are calculated as described in the text.

was obtained using a permeation device. The errors expressed on the graph are ±S.E.M. Sensitivities for the two represented concentration ranges are 28 ncps ppbv^{-1} for acetone below 50 ppbv and 3.7 ncps ppbv^{-1} for toluene between 150 and 1000 ppbv, where ncps means normalised (to 10^6 counts of hydronium) counts per second. The differences in sensitivities for the two molecules may arise from different transport properties through the mass spectrometer.

The sensitivity of the instrument can be calculated from the above data according to the expression [20]:

$$\text{sensitivity} = 10^{-3} \times \frac{kL}{\mu_0 N_0} \times \frac{N^2}{E} \tag{15}$$

where k is the proton transfer reaction rate constant, L is the drift tube length, μ_0 and N_0 are the reduced mobility and STP gas number density respectively, N and E are the drift tube gas number density and electric field. The above equation can be recast as:

$$\text{sensitivity} \propto L \times \frac{1}{(E/N)^2} \times E \tag{16}$$

from which it can be seen that sensitivity in PTR increases linearly with electric field and decreases with the square of the reduced field. Hence, a decrease in reduced field, combined with an increase in total FDT potential difference leads to an increase in sensitivity.

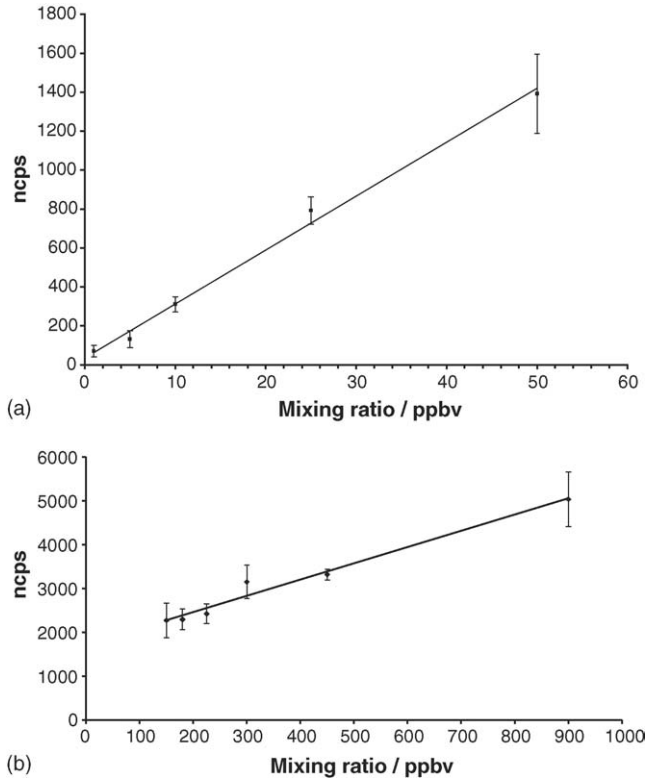

Fig. 10. PTR TOF calibration curves for (a) acetone; (b) toluene.

3.4. Resolution of nominal isobars

A significant advantage of ToF technology in tandem with PTR chemical ionisation is the ability of the mass filter to achieve high mass resolution compared to the commercially available PTR quadrupole analysers. Nominally isobaric molecules pose a difficulty in quantifying individual species in atmospheric analysis by conventional PTR. The quadrupole mass analyser identifies all nominally isobaric ions as the same mass, and hence reports potentially misleading mixing ratios if the presence of only a single species is assumed. This problem is exacerbated if the relative concentrations of the nominal isobars are changing rapidly. Mass resolution of nominal isobaric species solves this problem for non-isomeric isobaric species.

The mass accuracy of the PTR-ToF, as determined from six calibrated accurate mass measurements from 19 to 51 Th, is 264 ± 170 ppm. Mass calibration is achieved by interpolation from a graph of measured masses versus their known accurate masses (R^2 values better than 0.98). The mass reproducibility (as measured from 10 consecutive 1 min integrations) is <0.1%.

PTR-ToF spectra of ethanol (bottom trace of Fig. 11) and of a mixture of ethanol and methanoic acid (top trace in Fig. 11) were obtained using a permeation oven with nitrogen buffer gas. Mixing ratios of the two compounds are in the sub-ppmv range. Masses of protonated ethanol and protonated methanoic acid are 47.04969 and 47.01330 Da, respectively, requiring a resolution of 1290 ppm to distinguish between these two nominal isobars. Estimated FWHM for the peaks in the figure are 0.02 Th, and the measured separation of 0.023 Th (64% of the expected 0.036)

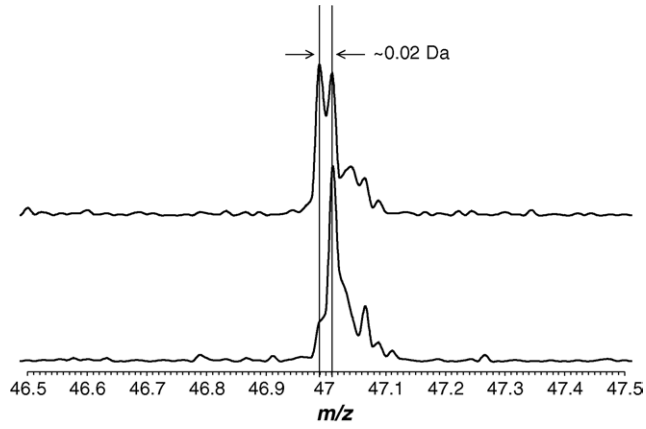

Fig. 11. PTR-ToF spectra of ethanol (bottom trace) and ethanol/methanoic acid mixture (top trace) showing mass resolution for the two compounds.

renders the peaks resolvable on the basis of FWHM separation. Resolution at this level is also capable of distinguishing between methanol and cationic $^{16}O^{17}O$, present in PTR spectra as a result of back diffusion of air into the discharge source, and demonstrates the potential of ToF MS for speciation of analytes in PTR MS.

4. Conclusions and future modifications

We have demonstrated the operation of our first generation hollow cathode PTR-ToF mass spectrometer. The instrument is capable of detection of a few ppbv of gaseous analyte on the order of a few seconds, with a sensitivity at this volume mixing ratio approaching 30 ncps ppbv^{-1} for acetone. The instrument response is linear over concentration ranges of important atmospheric trace gases. Use of a time-of-flight mass spectrometer, rather than quadrupole-MS, has offered the expected advantages including far superior mass resolution and multichannel data acquisition, allowing the capture of the complete mass spectrum over short timescales. These characteristics offer distinct advantages in the analysis of complex mixtures when compared to commercially available PTR-quadrupole-MS instrumentation. Unlike a similar PTR-ToF designed for field operation [15], our instrument also has the advantage that it operates without a radioactive ionisation source. At present, our sensitivity is approximately 5- to 10-fold less than the commercially available PTR-quadrupole-MS, however in this paper we have identified aspects of design modification which are expected to lead to enhanced performance. Installation of a venturi inlet on the ion injection orifice of the FDT is expected to lead to a favourable decrease in reduced field by allowing the operation of the drift tube at higher pressures and higher operating voltages. Reduction in reduced field is important in the present case due to the high population of fragmentation pathways which leads to complication of the mass spectrum of complex mixtures of analytes, and essentially reduces the sensitivity of the instrument by attenuating protonated molecule intensities.

Further potential advantages arising form the installation of a venturi orifice are an increased hydronium yield, an increased sensitivity, and a decrease in clustering (due to adjustment of the

water vapour/hydronium dynamic equilibrium). The increase in hydronium yield when the instrument is operating with air as the buffer gas arises from the limiting of back diffusion of buffer into the ion source, where dioxygen competes with water as a charge carrier in the hollow cathode plasma. Increased sensitivity arises from the potential to increase the drift tube pressure while maintaining constant a reduced field, the sensitivity being directly proportional to pressure at constant E/N as shown in Eq. (16). Also, attention to orifice geometry is expected to lead to further decreases in detection limit through increased ion transport through the FDT and into the ToF mass spectrometer.

These modifications are intended to constitute the second generation PTR-ToF, which we expect to yield higher sensitivities and lower limits of detection, leading to a portable instrument capable of rapid analysis of ultra trace components in the gas phase with high mass resolution.

References

[1] C. Waneke, J. Kuczynski, A. Hansel, A. Jordan, W. Vogel, W. Lindinger, Int. J. Mass Spectrom. Ion Proc. 154 (1996) 61.
[2] W. Lindinger, A. Hansel, Plasma Sources Sci. Technol. 6 (1997) 111.
[3] A. Hansel, A. Jordan, C. Warneke, R. Holzinger, W. Lindinger, Rapid Commun. Mass Spectrom. 12 (1998) 871.
[4] W. Lindinger, A. Hansel, A. Jordan, Chem. Soc. Rev. 27 (1998) 347.
[5] W. Lindinger, A. Hansel, A. Jordan, Int. J. Mass. Spectrom. Ion Proc. 173 (1998) 191.
[6] S. Hayward, C.N. Hewitt, J.H. Sartin, S.M. Owen, Environ. Sci. Technol. 36 (2002) 1554.
[7] C.N. Hewitt, S. Hayward, A. Tani, J. Environ. Monit. 5 (2003) 1.
[8] A. Tani, S. Hayward, C.N. Hewitt, Int. J. Mass Spectrom. 223–224 (2003) 561.
[9] A. Hansel, T. Mark (Eds.), Int. J. Mass Spectrom. 239 (2004) 77.
[10] First International Conference on PTR MS and its applications. http://www.uibk.ac.at/c/c7/c722/Tagungen/PTRMS03/proceedings_2nd_ed.pdf.
[11] Second International Conference on PTR MS and its applications. http://www.ptrms.com/publications/cont_2nd_conference.pdf.
[12] Y. Ikezoe, S. Matsuoka, A. Viggiano, Gas Phase Ion-Molecule Reaction Rate Constants Through 1986, Maruzen Company Ltd., Tokyo, 1987.
[13] J. Zhao, R. Zhang, Atmos. Environ. 38 (2004) 2177.
[14] P. Prazeller, P.T. Palmer, E. Boscani, T. Jobson, M. Alexander, Rapid Commun. Mass Spectrom. 17 (2003) 1593.
[15] R.S. Blake, C. Whyte, C.O. Hughes, A.M. Ellis, P.S. Monks, Anal. Chem. 76 (2004) 3841.
[16] D.A. Dahl, Int. J. Mass Spectrom. 200 (2000) 3.
[17] A.M. Howatson, An Introduction to Gas Discharges, 2nd ed., Pergamon, 1976.
[18] A.V. Tolmachev, I.V. Chernushevich, A.F. Dodonov, K.G. Standing, Nucl. Instr. Meth. Phys. Res. B 124 (1997) 112.
[19] T. Reiner, O. Mohler, F. Arnold, J. Geophys. Res. 103 (D23) (1998) 31309.
[20] J. deGouw, C. Warneke, T. Karl, G. Eerdekens, C. van-der-Veen, R. Fall, Int. J. Mass Spectrom. 223–224 (2003) 365.